Chapter-4

The Effect of Synthesis temperature on reduced graphene oxide ZnO nanocomposite and their photocatalytic performance with Phenolic Compound

4.1Introduction

Shape and size of photocatalysts such as ZnO are very important for photolytic activities. Research is now focused on obtaining this material in a definite microstructure like nano-rods, hollow microspheres, hexagonal, disks-flower type structures and nano-rings (H.Moussa, et al. 2016; Q. Yanget al.2010; T. Liu et al. 2015; K. P.Ghoderao et al. 2017; A. Shanmugasundaram, et al. 2018). Controlled morphology of ZnO also improves its chemical and physical properties with enhanced catalytic potency (K. P. Ghoderao et al. 2017). Crystal structure of ZnO is stacked by some of tetrahedral coordinated O^{2-} and Zn^{2+} ions alternately along the c-axis. Its structure is mainly of two inter connecting sublattices of Zn^{2+} and O^{2-} ions in such a way that Zn^{2+} ions occupy the position, which is surrounded by tetrahedral O^{2-} ions and its vice-versa also occurs. Therefore, it possesses two polar surfaces in which, one is positively charged (0 0 0 1) - Zn, and other is negatively charged (0 0 0 -1)-O. These surfaces are responsible for chemical activity (M.R.Parra, F. Z. Haque, et al. 2015).This type of tetrahedral coordination gives rise to polar symmetry along c-axis. This polar symmetry provides piezoelectricity and spontaneous polarization in ZnO crystals. It is also responsible for crystal growth and defect generation (Q. Li et al. 2010; J Tian, et al. 2012). It is well established now that ZnO possesses high surface reactivity and photosensitivity (J.Tian,et al. 2012; E. Poulios I. Micropoulou, et al. 2012). ZnO particles are optically sensitive, which produce hydroxyl radicals of strong oxidizing agents upon exposure to UV light (A.Khataee, et al. 2014). As a

single material, it shows less photocatalytic stability during light irradiation and therefore, limited the use of pure ZnO as photocatalyst (Q.Xiang, et al.2011; Y.W. Heo, et al. 2004). It is essential to improve its e-h pair separation efficiency for better photocatalytic activity. Research shows the photocatalytic activity of ZnO can be increased with other suitable materials (S. Gayathri, et al. 2014; Y.Bessekhouad et al. 2014). These materials are low band semiconductors, noble metals, and carbon materials (H.R. Pant, et al. 2012; A.S.Prasad, et al. 2015). The carbon-related materials have excellent photocatalysts properties and can be used in the degradation of organic pollutants (N. Zhang, et al. 2012; T. Lv, et al. 2012). Graphene in the form of reduced graphene (rGO) has better electronic properties (K.I. Bolotin, et al. 2008) and is a better option for photovoltaic, super-capacitors and fuel cells (X. Li, et al. 2009; Lee C., et al.2008). However, as single rGO, it possesses weak photocatalytic activity, but their composite with a combination of ZnO shows excellent photocatalytic activity (T. Xu, et al. 2011; Y. Bu, et al. 2013). In this connection, the morphology of ZnO is very important (E. Rokhsata, et al. 2016; R. Beura, et al. 2017; J. Qin,et al. 2017;S.He, P.Hou,et al. 2018; Wang Q., et al. 2018; R.Yadav, et al. 2019).

In previous studies, there are several reports on the synthesis of flower-like morphology of metal oxides such as ZnO, TiO_2, and SnO_2 (X. Zhao,et al. 2014; J.A. Quek,et al. 2018; Z. Ning,et al. 2019; Z.Lin et al. 2018; Z.Wu, et al. 2019; L.Yosefi, et al. 2019). However, most of these reports are concerned with different structures with toxic reagents or expensive substrates.Thus; there is a need to develop a method for the preparation of particular morphology that avoids toxic reagents and substrates. For this, the morphology of ZnO is of great interest due to its unique

structural dependence than other metal oxides (Z. Ning,et al. 2019).

As the controlled growth morphology of ZnO is particularly interesting and it has additional functionality, flower-like morphology has stimulated a great deal of interest which has potential for used in various fields (X. Zhao,et al. 2014;J.A. Quek,et al. 2018;Z. Ning,et al. 2019;W. Long,et al. 2017).There are different processing routes for the synthesis of ZnO nanoparticles such as sol-gel method (D.Richard et al. 2018; Z.Durmus,et al. 2019), hydrothermal method (J.Ding,et al. 2015), assisted solution route (M. Darwish,et al.2016) and aqueous chemical route (M. R. Parra, et al. 2014). Among them, the sol-gel method comprises lower complexity, low cost, a high degree of purity and more possibility to obtain lotus-like structures compare to the other synthesis method.

In the present work, we report for the first time, rGO-ZnO (in short form RZ) composites with lotus-like morphology of ZnO, prepared from aqueous ammonia through sol-gel method. The effect of temperature (60-100^{0}C) during synthesis was also investigated. Moreover, the photocatalytic activities of phenolic compounds had also been studied. The results showed that lotus-like morphologies in the temperature range of 70^{0}C to 90^{0}C could be obtained. The RZ composites, synthesized at temperature 70^{0}C, exhibited superior photocatalytic activity as compared to other samples. Further, the degree of degradation of the phenolic compound reaches up to 86% in 20min. The effects of surface morphology, surface defect and surface area of rGO in composites were also observed to study the degradation rate.

4.2 Results and Discussion

4.2.1 Reaction mechanism

In the experiment, when the solution of 0.01M $ZnSO_4.7H_2O$ was heated at 280^0C, it gets converted into zinc sulfate and water by thermal decomposition (J. Straszkoet, al.1997) according to Eqs. (4.1-4.3). It gets further converted into $[Zn(NH_3)_4]^{2+}$ due to zinc ammonia complex reaction with diluted ammonia solution. Finally, it formed zinc hydroxide $[Zn(OH)_2]$ as shown in the following reactions: -

$ZnSO_4.7H_2O \rightarrow ZnSO_4.6H_2O+H_2O$---------- (4.1)

$ZnSO_4.6H_2O \rightarrow ZnSO_4.H_2O +5H_2O$---------- (4.2)

$ZnSO_4.H_2O \rightarrow ZnSO_4+H_2O$---------- (4.3)

$ZnSO_4 +NH_3 \rightarrow [Zn(NH_3)_4]^{2+}$ ---------- (4.4)

$[Zn(NH_3)_4]^{2+}+ H_2O \rightarrow Zn(OH)_2+ 3NH_4OH$---------- (4.5)

When $Zn(OH)_2$ and GO mixed solution was heated at 60^0C, 70^0C, 80^0C, 90^0C and 100^0C respectively; the Zn^{2+} and OH^- ions produced according to Eq.(4.6). Zn^{2+} ions were now loosely bonded with rGO structures and formed COO-Zn^{2+} as shown in figure 4.1. When the concentration of Zn^{2+} and OH^- reached to the supersaturating degree of ZnO, ZnO nuclei were formed according to Eq.(4.5). Further, the growth units of $[Zn(OH)_4]^{2-}$ were formed according to Eq.(4.8). In the solution, rGO sheets provided numerous negatively charged sites which possibly attracted the positively charged Zn^{2+} ions and became nucleation sites for ZnO formation. The mechanism of lotus-like ZnO synthesis with rGO can be explained by following reactions and figure 4.1:-

$Zn(OH)_2 + GO \rightarrow Zn^{2+} + 2OH^- + rGO$---------- (4.6)

$Zn^{2+} + 2OH^- + rGO \rightarrow ZnO + H_2O + rGO$---------- (4.7)

$Zn(OH)_2 + 2OH^- + rGO \rightarrow [Zn(OH)_4]^{2-} + rGO$----------(4.8)

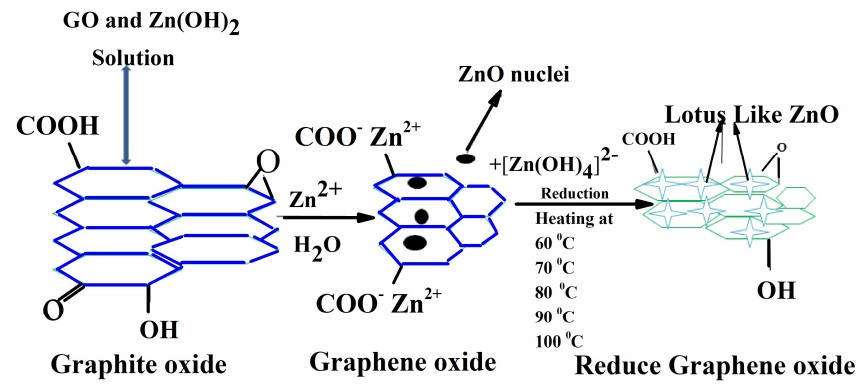

Figure 4.1 Growth mechanism of inverted and non-inverted lotus-like ZnO morphology with reduced graphene oxide.

4.2.2 Characterizations of Materials

Reduced graphene oxide (rGO) was synthesis by using the modified Hummers Hoffman method (W.S.Hummers 1958) with graphite powder as the starting material. The synthesis method of rGO has been discussed in chapter-3 (section-**3.4.1).** The sample of reduced graphene oxide (rGO) was coded by rGO. The lotus- like morphology of ZnO with rGO, synthesized by sol-gel method at different synthesis temperature. The synthesis method of lotus- like ZnO-rGO has been discussed in chapter-3 (section-**3.4.2)**. The samples were coded as RZ60, RZ70, RZ80, RZ90 and RZ100 respectively. Figure 4.2 (a) shows the XRD patterns of the RZ70, RZ80, RZ90, and rGO. The peaks in the range of 10-30^0 are represented by peak marked as '∆' with their millar indexed plane and shows similar to that of carbon black (T.V. Cuong, et al.2010), and peak between 20-30° indicates the

restacking of the reduced graphene sheets (H.L.F. Eduardo,et al. 2007; H.P. Cong et al.2010, E. Falcao,et al.2007;Y.Zhao,et al.2017, A.F.Betancur, et al.2018). Reflection planes of the 'Δ' peaks have been mached with the standard JCPDS card no 41-1487 (shown in appendix-1) and listed in appendix-4&5. These deviate from the characteristic (002) peak of the pristine graphite. The small bumpsin samples RZ70, RZ80, RZ90 and rGO in range of $10\text{-}30^0$ are also shown in the inset of figure 4.2 (a).The intensityof a small bump in the sample RZ70 is higher than compared to the sample RZ80, and this bump disappeared in the sample RZ90. The peaks in the range of $10\text{-}30^0$ indicate that the GO is not completely reduced and hence it can be concluded that the chemical reduction always results in the presence of few defects and residual oxygen moieties. ZnO is represented by peak marked '**Θ**' with their indexed plane according to standardized JCPDS No.36-1451 of ZnO and shown in figure 4.2 (a). From this figure reflection planes at different anggle for the sample RZ70, RZ80 and RZ90 have been mached with the standard JCPDS card no 36-1451 (shown in appendix-2) and listed in appendix-6, 8 & 9. The major plane (101) of RZ composite is significantly present, while other peaks having (hkl) values (100), (002), (101), (102) (110), (103), (200), (112), (201), (004) and (202) are observed with comparatively lower intensities.These can be indexed to crystalline hexagonal wurtzite structure according to the standardized JCPDS No.36-1451 of ZnO. However, no characteristic peaks were observed for either GO or graphite in the corresponding region. This could be due to the transformation of GO to rGO. No characteristic peaks of other impurities such as $Zn(OH)_2$ were detected in the XRD patterns. Figure4.2 (b) and its inset showed the relative intensity increase for the peaks corresponding to the (002) with the increase in synthesis temperature without

effecting the content of rGO. This is due to the increasing crystalline nature of ZnO nanoparticles with increasing temperature.The results indicated the preferred orientation along c-axis, resulting in the growth of nanoparticles along the [001] direction (Y.Chenet al.2009; M.Azaranget al.2014).This result is also agreement with the HR-TEM results. The crystalline sizes, corresponding to the plane (101) were estimated by employing Deby-Scherrer formula (B.D.Cullity et al.2001).The lattice parameters corresponding to the (100) and (002) plane orientations were calculated (D.Fu, G.Han, et al.20012). The lattice contants and estimated error bars (±σ) of measured lattice contants, "a" and "c" for all samples are listed in able 4.1. The crystalline size for all samples is also listed in table 4.1. The calculated lattice constants are in good agreement with JCPDS card 36-1451(table 4.1). From the data listed in table 4.1, the crystallite size of RZ70 is smaller than RZ80 and RZ90. From this table, it was found that the lattice contant and crystallite size changes in different composites due to the presence of rGO (D.Fu, G.Hanet, al.2012). It is also found that the crystallite size in the case of RZ80 and RZ90 does not change due to the similarity in peaks broadening of ZnO peaks (F.Zahedi, et al.2014, P. Sengunthar et al. 2020). From the table 4.1 the cell volume of the sample RZ70, RZ80 and RZ90 are varying with increasing the synthesi temperature. It is minimum for RZ80 than RZ70 and RZ90 due to variation of the lattice contant (B. Rajesh Kumar, et al.2017).

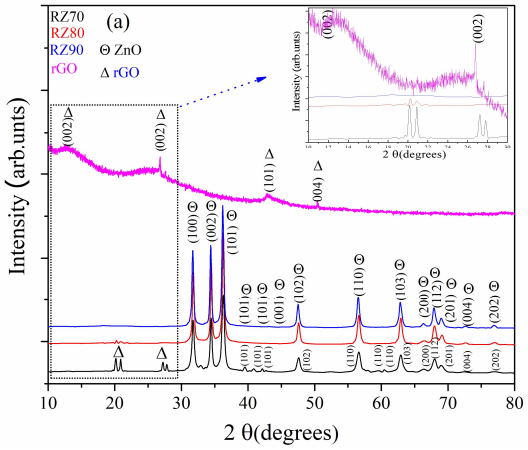

Figure 4.2 (a) XRD Patterns of low temperature synthesized RZ composites that were grown at 70^0C, 80^0C, and 90^0C respectively.

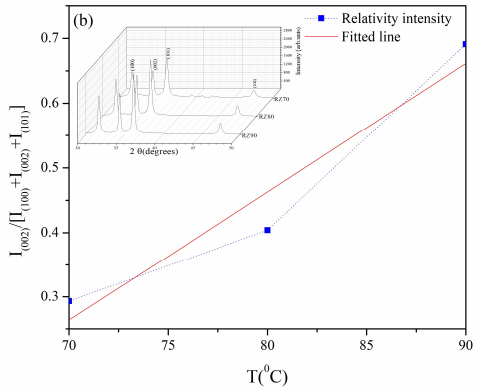

Figure4.2 (b) Relative intensity (inset) and the relative intensity of (002) peaks vs. synthesis temperature of RZ70, RZ80 and RZ90.

Table 4.1 The physical properties of the lotus structure of ZnO in RZ composites prepared in this work.

Sample	Unit cell Parameters			Crystalline size(nm)	Cell volume(A^0)^3	E_g(eV)
	a ±σ [A^0]	c ±σ [A^0]	c/a ±σ [A^0]			
RZ70	3.255±0.005	5.2051±0.0019	1.599±0.0019	20	47.76	3.17
RZ80	3.226 ±0.024	5.2022±0.0048	1.602±0.0019	28	46.88	3.16
RZ90	3.258 ±0.008	5.213 ±0.0048	1.600±0.0019	28	47.92	3.16
Card	3.250	5.207	1.6021			

The crystal size calculated by plane (101), a and c are lattice parameters calculated on the bases of plan (100) and (002), the energy band gap E_g is obtained based on the absorption spectroscopy.

Figure 4.3 (a) shows morphologies of RZ60 in which growth of ZnO were observed as in an irregular manner. Figure4.3 (b) shows the morphology of RZ70 with increasing magnification. Lotus-like ZnO morphology with variable sizes in micrometer range is particularly seen as an inverted shape of a natural lotus and begins to form at temperature 70^0C. The morphology and many kinds of flower-like architecture of metal oxide have been reported (X.Zhao, et al. 2014; J.A. Quek, et al. 2018, Z.Ning, et al. 2019; Z.Lin, et al. 2018; Z.Wu, et al. 2019; L.Yosefi, et al. 2019). In this study the growth of flower-like architecture strongly depends on the concentration of Zn^{2+} and OH^- ions and involves the nucleation, growth, orientation and self- assembly of ZnO nanoparticles. In our work, rGO sheets are well dispersed in composite solution and provided numerous negative charged sites, which possibly attracted the positively charged Zn^{2+} ions (J. Mao, et al. 2017) and resulted in the formation of ZnO crystal precipitates.

The precipitate, obtained at the processing temperature of 70^0C was containing a large number of nanorods. The surface energy of individual nanorods was quite high due to its surface to volume ratio, and they have surface charges also. This resulted in their self-assembly and showed numerous ZnO nanorods with minimizes surface energy and unity at one junction, just forming natural lotus-like structure. In another observation as shown in figure 4.3(c), the morphology of RZ80 is straight natural lotus (non-inverted)-like structure. The change of inverted lotus-

like morphology into straight lotus- like morphology may be due to the rise in reaction temperature. With an increase in reaction temperature, the assembly of inverted lotus-like morphology is randomized, which are self-assembly together to form non-inverted lotus- like morphology.A typical EDX spectroscopy of the product obtained at temperature 80^0C is also shown in the inset of the figure 4.3(c). Here carbon, zinc, and oxygen are the only detectable elements without any contamination. The figure 4.3 (d) shows the morphology of RZ90 with further changes as compared to the morphology of RZ70 and RZ80. Figure 4.3 (e) shows the morphological of the RZ100. In this image, the morphology is particularly distorted from a lotus-like structure.

It can be predicted from results that synthesis temperatures have influenced the growth orientation of ZnO microstructures. The increase in the temperature during synthesis from 60-100^0C has changed the structural morphology. The structural morphology of ZnO in the composites at temperature 70^0C is well-formed lotus-like structure. This type of structure further changes with the increase in temperature and disappears at 100^0C. It may be due to dehydration of $Zn(OH)_4^{2-}$ ions (W.J. Li,et al. 1999) in the chemical reaction when the precursors are heated beyond the temperature range of 70-90^0C. This can also be concluded that ZnO nanoparticles do not self-assembled as lotus-like at 60^0C due to low energy for stabilization of nanoparticles while at 100^0C, the energy is high for stabilization of nanoparticles. So, it is confirmed that there is a considerable effect of synthesis temperature on the morphology of ZnO.

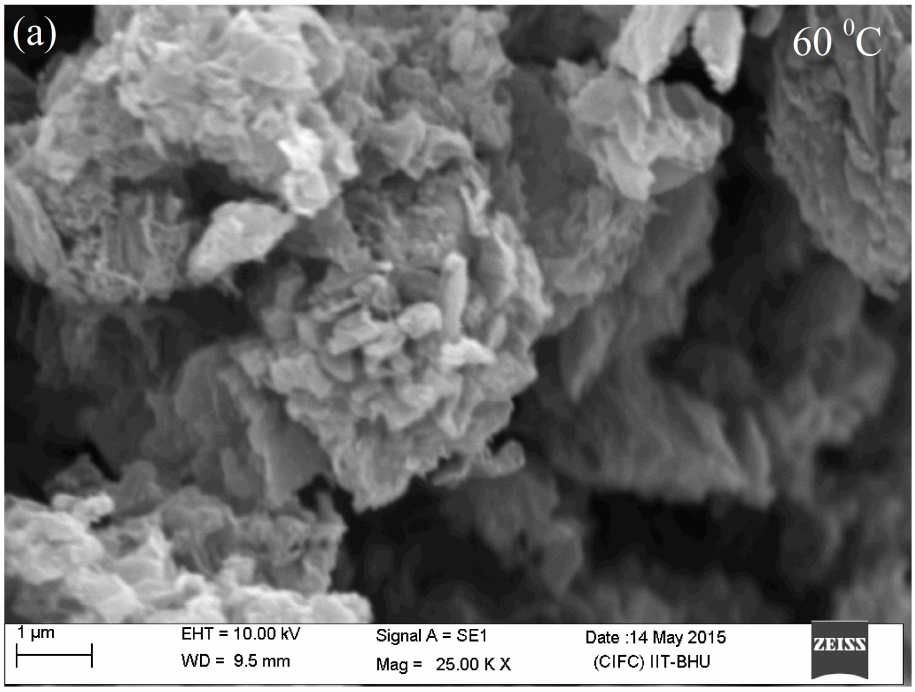

Figure 4.3 (a) SEM images of RZ composites at temperature 60^0C.

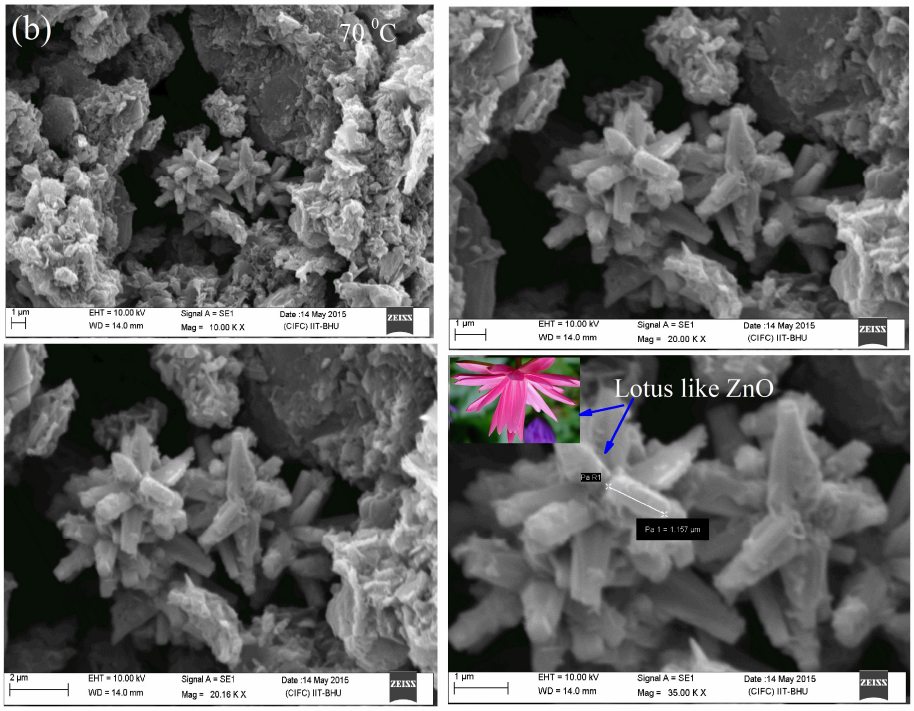

Figure 4.3(b) SEM images of RZ composites at temperature 70^0C with increasing magnification.

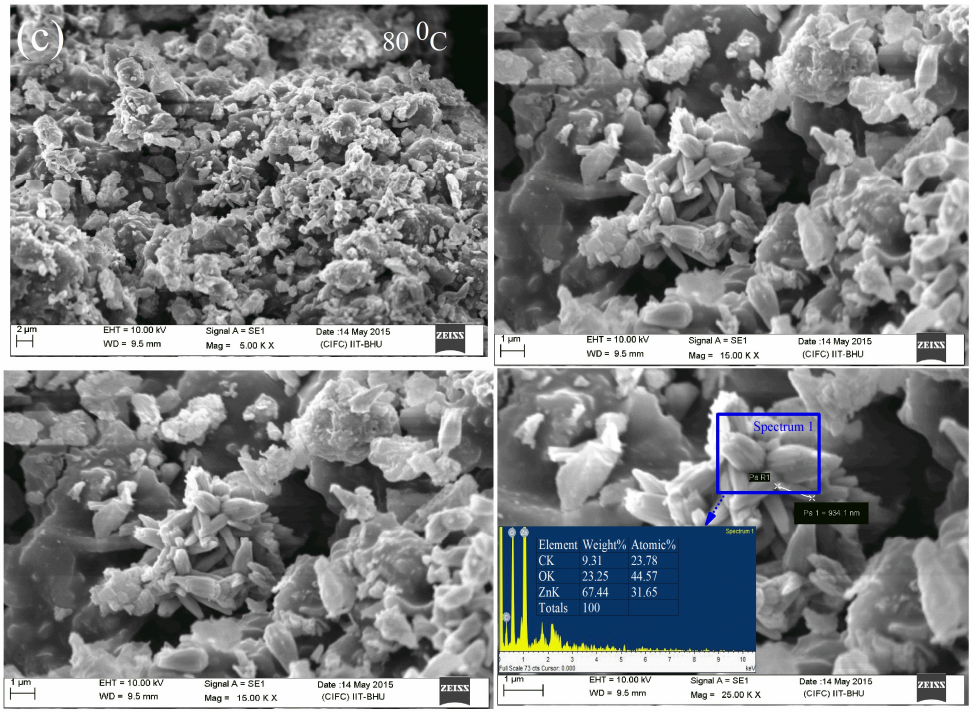

Figure 4.3(c) SEM images of RZ composites at temperature 80^0C with increasing magnification and with EDX pattern.

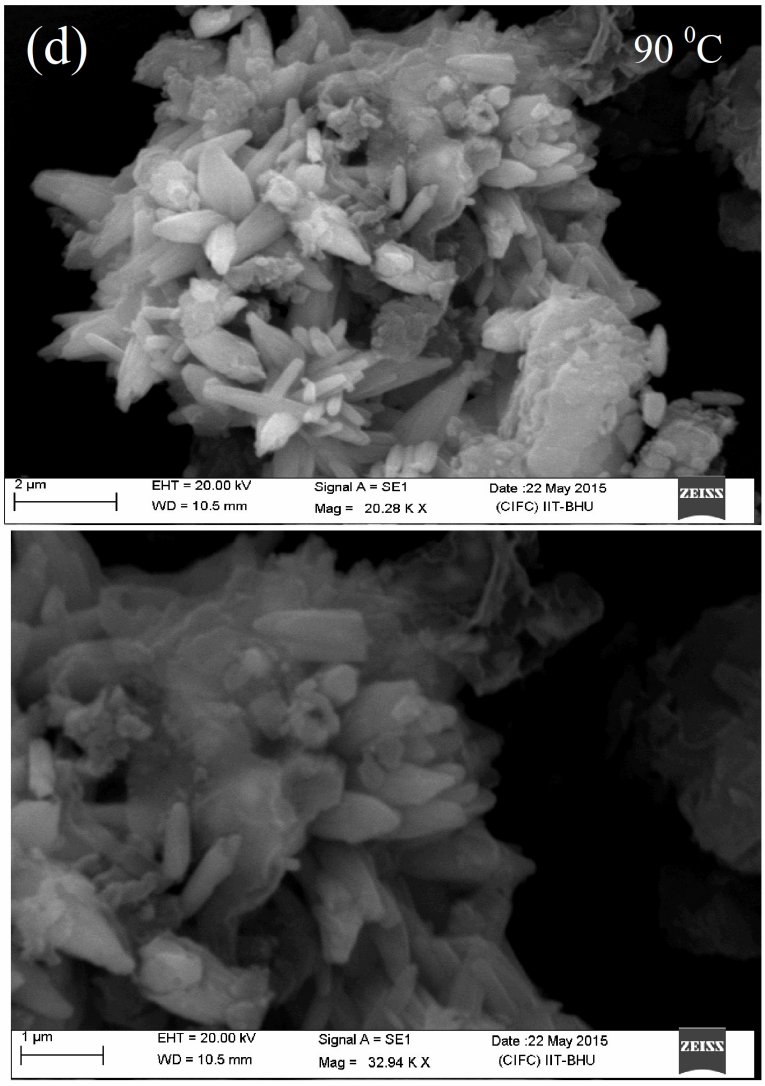

Figure4.3 (d) SEM images of RZ composites at temperature 90^{0}C with increasing magnification.

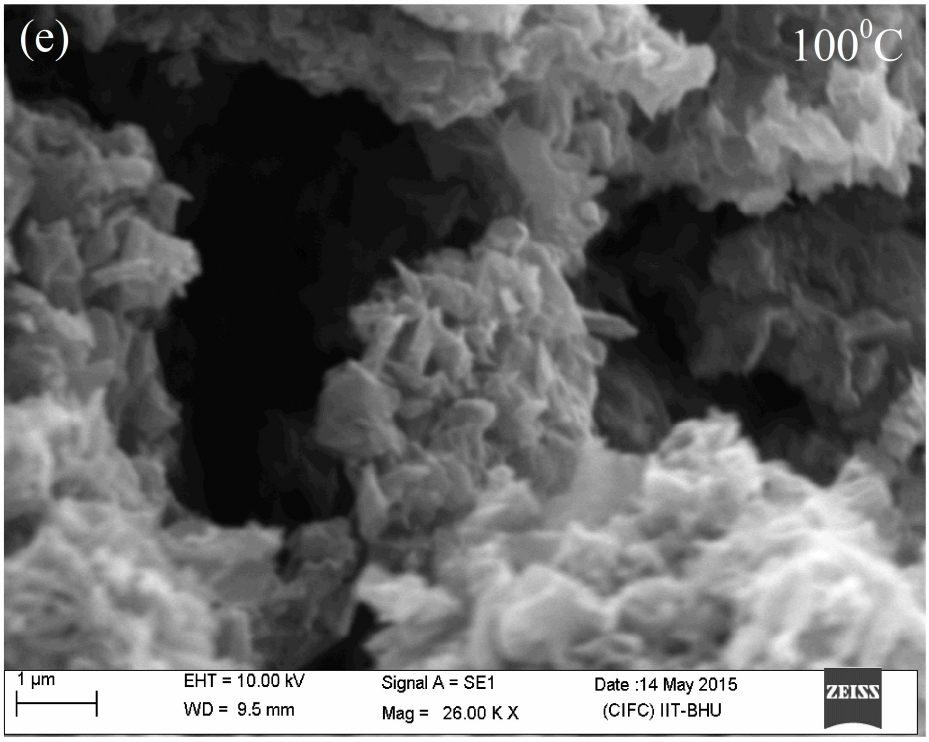

Figure 4.3(e) SEM images of RZ composites at temperature 100^{0}C with increasing magnification.

Figure 4.4(a) & (b) shows the HR-TEM image of RZ80 with increasing magnification. The dark section represents ZnO and indicated by arrow. The distribution of lotus-like ZnO over the rGO sheets can be seen as a leaf-like structure. Some structures are also covered with rGO sheets. This behavior indicates that ZnO and rGO make strong electronics interaction and improve the charge separation, resulting in increased photocatalytic activity. The SAED pattern of RZ composite as shown in figure 4.4(c) can be used to determine the crystalline properties of RZ composites. The SAED pattern shows the specific crystalline plane of ZnO. From the SAED pattern, the spacing between two successive rings through image j software was measured, and its reciprocal value is equal to the lattice spacing (d). For all successive rings, lattice spacing was also calculated similarly. These values were

consistent with the XRD results. From SAED pattern observations, the lattice spacing corresponding to the plane (002) was approximately 0.256nm. This value is approximately equal to the value reported in the literature by Majit Azarang, et al. 2014. It is concluded here that nanoparticles of ZnO preferred orientations along the c-axis and were grown along [001] direction.

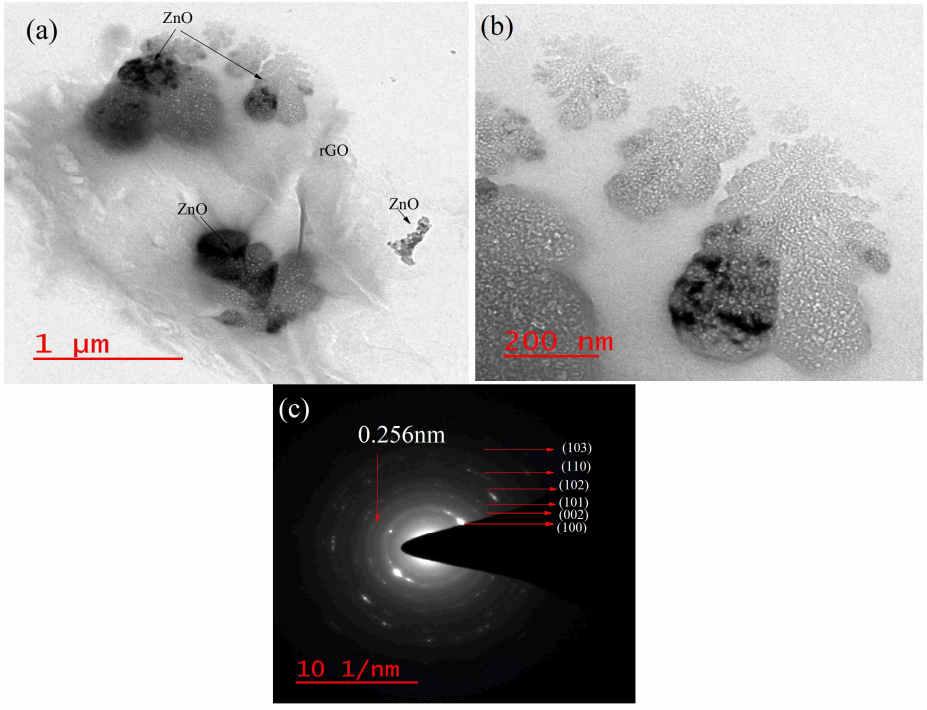

Figure 4.4 HR-TEM images of RZ80 with increasing magnification labeled by leaf like, in inset was the SAED pattern of ZnO.

Figure 4.5 shows the UV-vis absorption spectra of RZ70, RZ80, and RZ90 composites. The GO sheets demonstrated an absorption peak, centered at 270nm and a shoulder at about 300nm. It was observed that there was maximum absorption in RZ80 as compared to the RZ70 and RZ90. The optical band gap of RZ70, RZ80, and RZ90 were determined by extrapolating the linear region of the $(\alpha h\upsilon)^2$ versus energy plots as shown in the inset of figure4.5. The resultant optical band gap energies (E_g) are listed in table 4.1. From this table the crystallite size of RZ70 is smaller than

RZ80 and RZ90. In this regard, according to quantum confinement theory, the enery band gap of semiconductor depends on the crystal size; its value will increase with a decrease in crystal size. Hence the enery band gap of RZ70 is increased than RZ80 and RZ90 due to quantum confinement effect. It was also found that the value of E_g of RZ70,RZ80 and RZ90 was decreased as compared to the bulk band gap energy of pure ZnO (E_g~3.2).The decrease in band gap energy of pure ZnO is due to variation of ZnO morphology and rGO content. In this regard various lattice may be associated atomic interection phenomena come into play from its ionic crystalline lattice nature which is reduced the enery band gap of pure ZnO (L.C.Nehru et al.2012, J.Gonioakowski et al. 1995). It is also due to transfer of the photogenerated electron from ZnO to rGO in composites (Ch. Rodwihok, et al.2019, S.Abdolhosseinzadeh, et al. 2015). This indicated the formation of Zn-O-C chemical bond in composites (H.Zhanget al.2009). The result shows that the electronic structure of lotus-like ZnO microstructures was slightly varied in the electronic structure of bulk ZnO due to the absence of confinement effects in nanometer sizes. Figure 4.6 shows two distinct sharp emission peaks at wavelength 402nm and 426nm respectively. The broad band at 450-600nm can also be shown in the inset of figure 4.6.The peak at 402nm arises because of near-band-edge emission and the peak at 426nm arises due to the electronic transition (electron-hole pairs). The broad range emission band at around 450-600nm originated from the deep-level transition in the surface defects (R.Agrawal et al.2011; L.S.Zhong, et al.2008; H.B.Kimet al.2016). The PL peak intensities at wavelength 402nm and 426nm were maximum for the composites RZ80 and minimum for composite RZ90. However, in the broad band range, the intensities were maximum for RZ80 and minimum for composites RZ70.PL intensity

of the RZ composites decreased significantly which may be due to the enhanced separation rate of photoinduced charge carriers by effective charge transfer from the ZnO to the rGO and also due to the morphological variations of composites as depicted in SEM results. The broad band peakat 560nm was weaker than the peaks at 402nm and 426nm. These may have resulted from the presence of GO which may provide a favorable effect of eliminating the defect of the ZnO particles or can accept the photo-generated electrons (D. Fu, G. HanG., et al.2012).

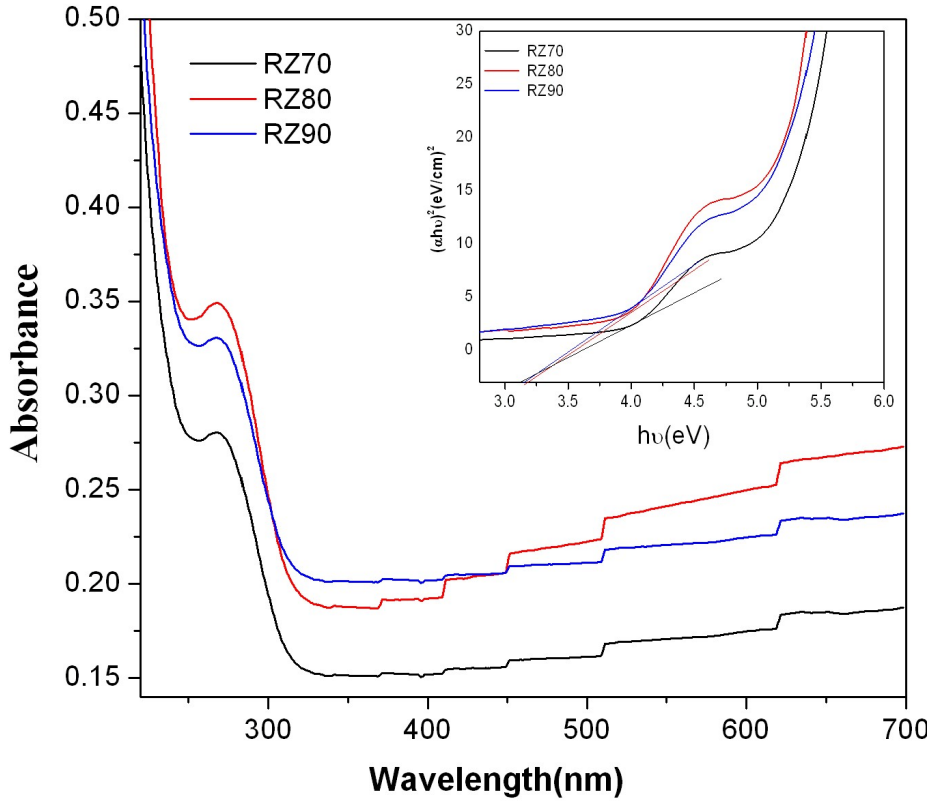

Figure 4.5 UV-visabsorption spectra of RZ70, RZ80 and RZ90 composites and with their extracted optical band gap in the inset.

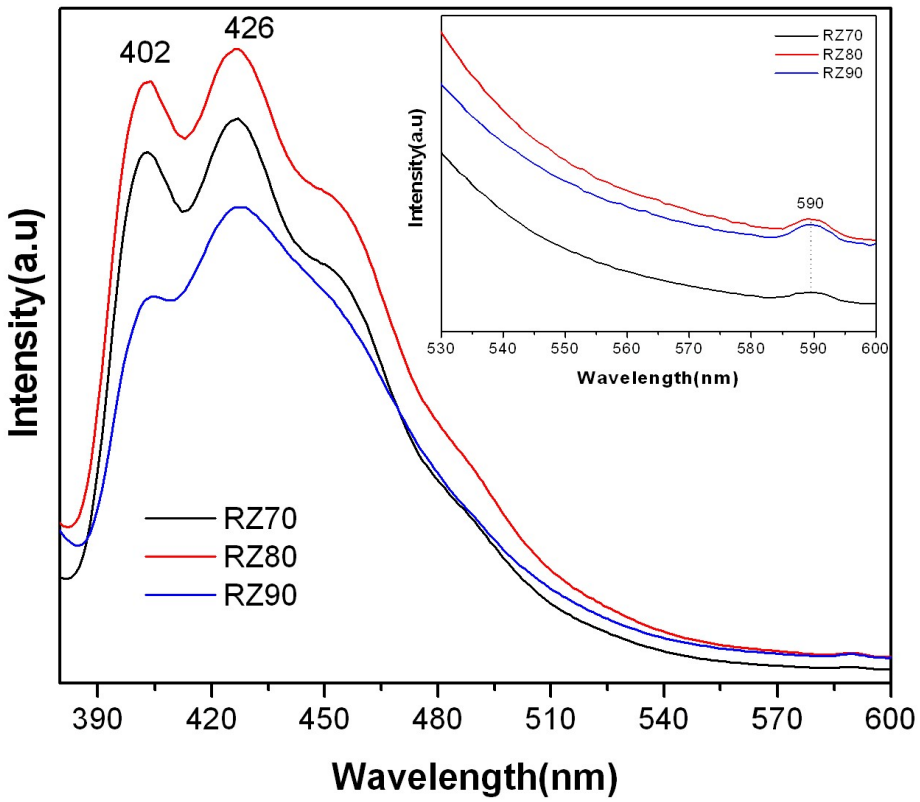

Figure 4.6 PL spectra of RZ70, RZ80 and RZ90.

Figure 4.7 shows FTIR spectra of RZ70, RZ80, and RZ90.The band at 3424cm^{-1} signified the hydroxyl groups of absorbed H_2O molecules. The carboxylic groups at 1431cm^{-1}, hydroxide group at 1260cm^{-1} appeared in RZ70 and RZ90 but disappeared in RZ80. This result indicated that some of them disappeared after the reduction treatment, indicating the absence of most of the functional groups. The peak at 460cm^{-1} represented the sample having Zn-O bonds (N.Lepot,et al.2007).

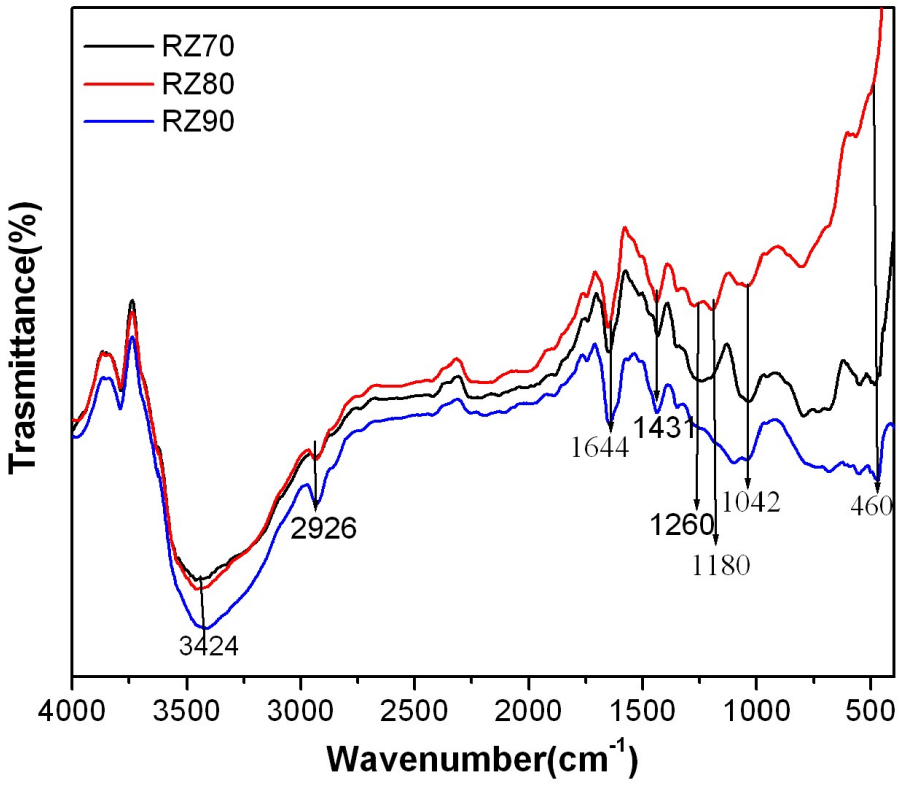

Figure 4.7 FTIR spectra of RZ70, RZ80 and RZ90.

Figure 4.8 shows the Raman spectroscopy of composites RZ70, RZ80, and RZ90.There are two prominent peaks at 1320cm^{-1} (D- band) and 1570cm^{-1}(G- band) along with another peak at 2625cm^{-1} (2D- band).The D peak is due to the existence of first-order zone boundary phonons defected graphene and the G peak corresponding to the breathing mode. The intensity ratio of D band to G band can be utilized for judging the degree of disordered/ordered of carbon nonmaterial (A.C.Ferrari,et al.2006).The 2D band originates from a two-phonon double resonance (M.Mohandosset al.2017).The D and G peaks of rGO appear at around 1321 cm^{-1} and 1568 cm^{-1} and represent sp^3 and sp^2 clusters inside rGO structure(Abid et al. 2018).The presence of the 2D band in RZ70 and RZ90 confirmed that RZ70 and RZ90 have more graphitic structure than RZ80. It was also

observed that G peaks of the sample RZ80 shifted towards a higher wave number as compare to the samples RZ80 and RZ90.The shift in the G band has suggested a reduction of GO to rGO. The intensity a ratio of the D to G band (I_D/I_G) is known as a measure of the size of sp^3 /sp^2 domains in rGO) sheets and determines the band-gap in rGO sheets (Abid et al. 2018). The intensity ratios of the D to G band (I_D/I_G) were calculated as 0.8414, 0.8220 and 0.8395 for RZ70, RZ80 and RZ90 respectively, as shown in figure 4.8.The I_D/I_G value of RZ70 was larger as compared to RZ80 and RZ90, indicating more defects and disorder in RZ70 in carbon material (A. Merlen et al.2017). The band-gap of rGO is equal to 0.8414eV of our synthesis sample which is also indicates the reduction of GO.

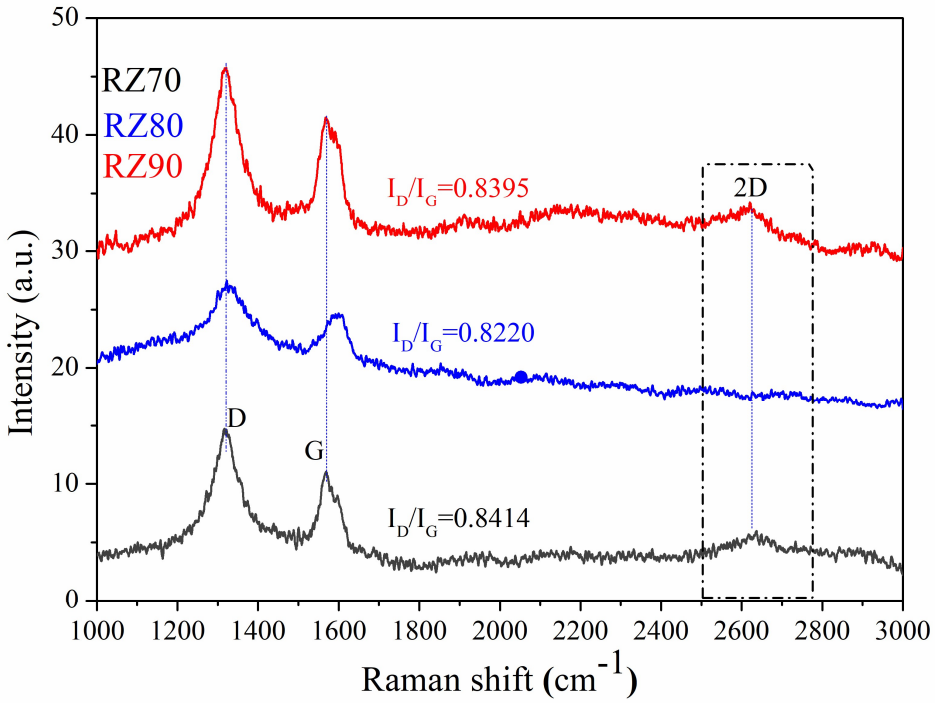

Figure4.8 Raman spectrum of RZ70, RZ80 and RZ90.

4.3.3 Photocatalytic degradation activities of RZ nanocomposites with phenol

Figure4.9 (a-c) shows the photodegradation of phenol using composites RZ70, RZ80 and RZ90 as a catalyst. In the absence of the catalyst, very little change in the UV-visible spectra was observed. Figure4.9 (a-c) exhibits an absorption peak at 262nm. The intensity of this peak decreased with an increase in exposure time of sunlight. A slightly variation in peak value for RZ80 and RZ90 was also observed as shown in figur4.9 (band c) because of the similarities in the morphology of the composites.

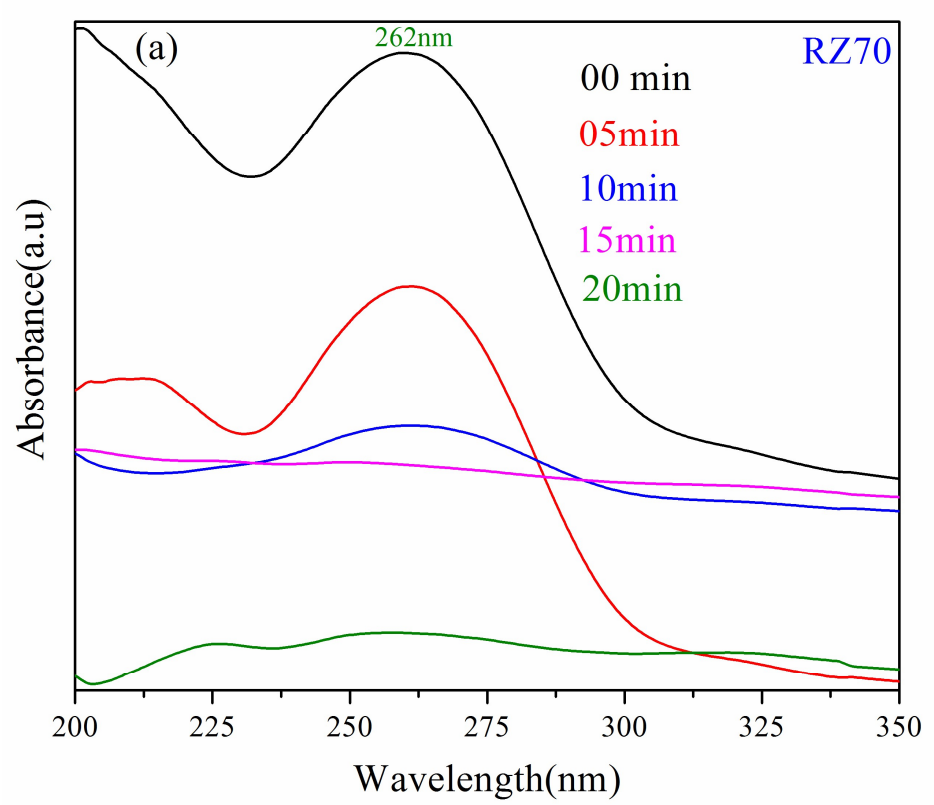

Figure 4.9 The time-dependent UV-Visible absorption spectra of phenol in the presence of catalysts (a) RZ70.

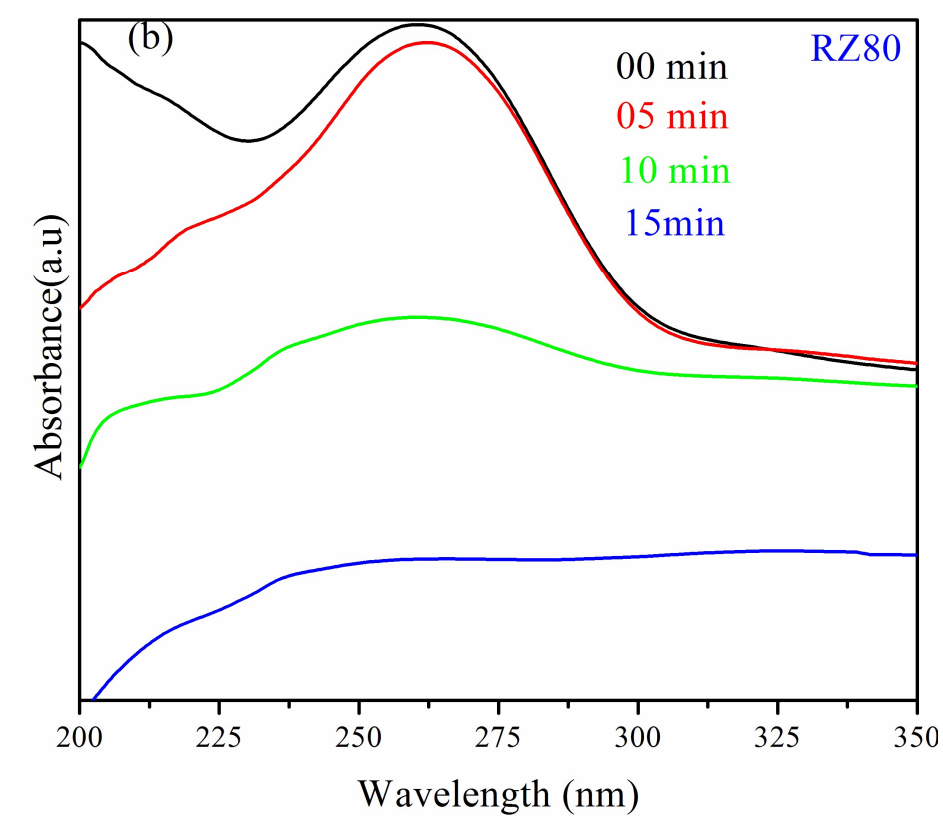

Figure 4.9 the time-dependent UV-Visible absorption spectra of phenol in the presence of catalysts (b) RZ80.

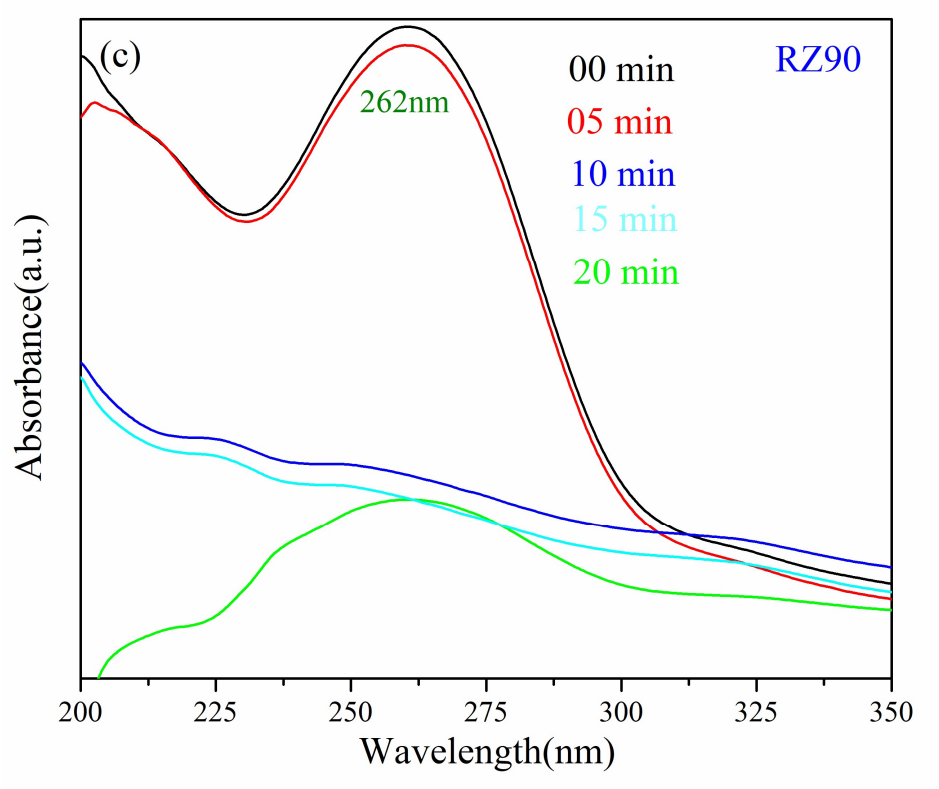

Figure 4.9 the time-dependent UV-Visible absorption spectra of phenol in the presence of catalysts (c) RZ90.

The concentration ratio (C/C_0) was varied during the photocatalytic experiment and showed the dependency on the maximum absorbance ratio (A/A_0) as shown in figure 4.10 (a) along with its inset. The concentrations of RZ70, RZ80, and RZ90 were gradually decreased with increasing time, indicating the enhanced degradation efficiency.Figure4.10 (b) and its value in inset show a comparable percentage degradation curve for all the catalysts with phenol. It was observed that degradation efficiency of phenol after 15min was 81%, 75% and 74% of RZ70, RZ80 and RZ90 respectively.It was also observed that the degradation efficiency increases on increasing irradiation time which indicates the residue of phenol decreased. It was

due to the sufficient energy available for the reaction of the molecules. Another reason may be due to catalytic activity with increasing irradiation time.The enhancement of photocatalytic performance using RZ70, RZ80 and RZ90 were due to the morphology and structural defect in ZnO such as oxygen vacancies, Zinc vacancies, oxygen interstitials and Zinc interstitials (H.N.Tien, et al.2013) with the surface defect of rGO (S.K.Mandals et al.2019) in RZ catalyst.The maximum degradation efficiency was achieved for the sample RZ70. It can be predicted that the morphology of sample RZ70 was best for the degradation of phenol. Figure4.10(c) shows the recycled use of RZ70, RZ80, and RZ90 for five times. There was a slightly effect the degradation efficiency, and it can be concluded that these composites can be reused. This is due to the photo-corrosion effect of ZnO (Y.C. Liang, et al.2017).

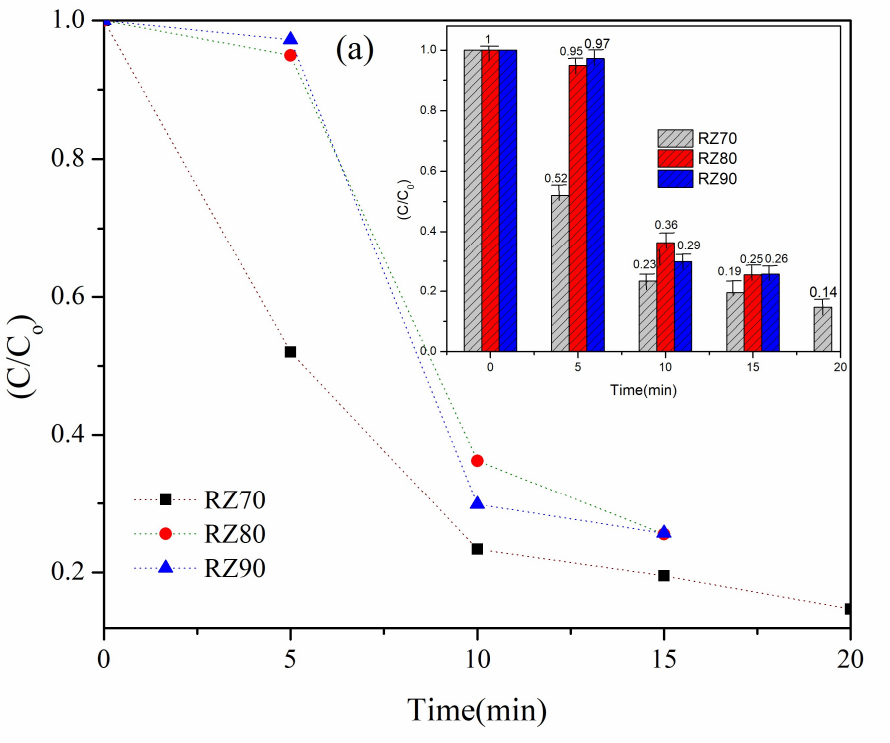

Figure 4.10 (a) photocatalytic degradation of phenol with time under sunlight irradiation and with their degradation value in the inset.

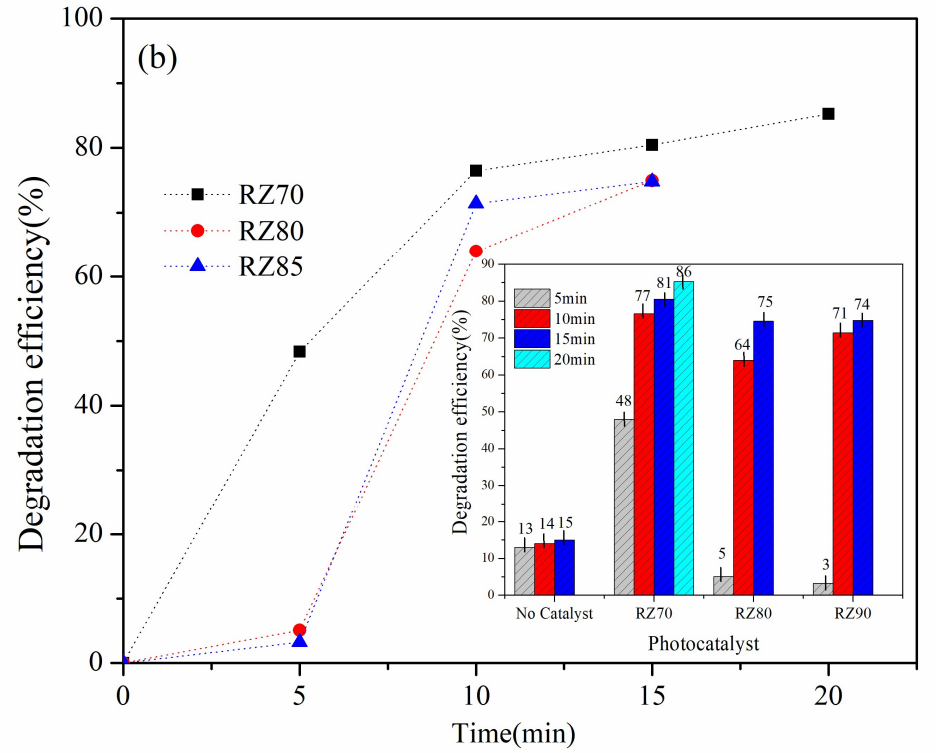

Figure 4.10(b) Comparison of the photocatalytic degradation efficiency of the photocatalyst towards phenol with their degradation value in the inset.

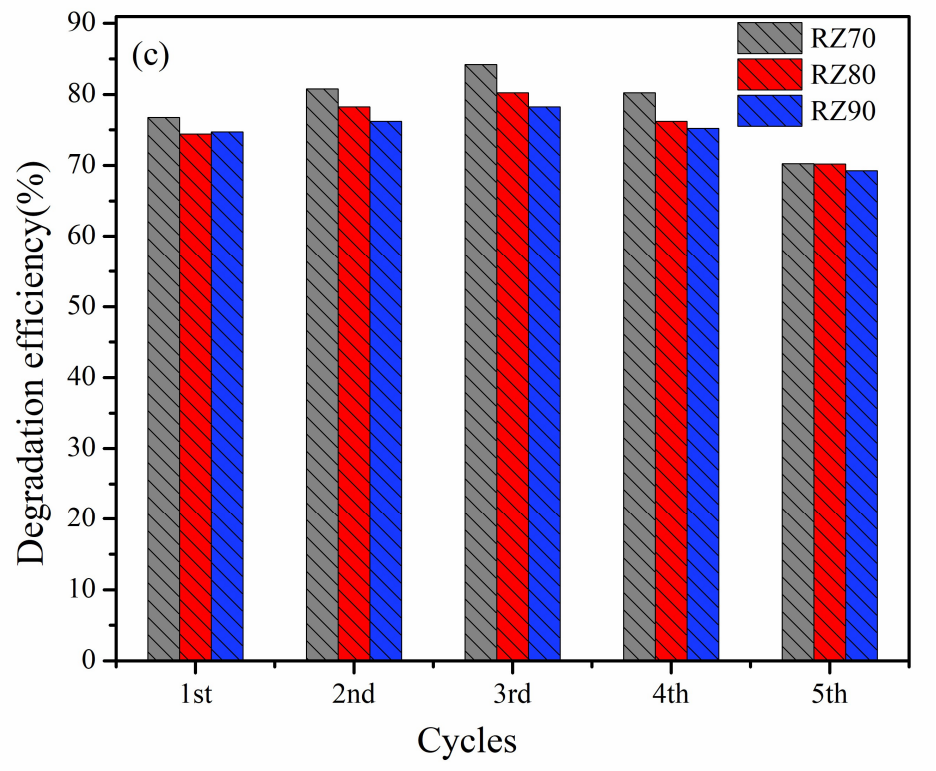

Figure 4.10 (c) Reusability study of RZ70, RZ80 and RZ90 nanocomposite for degradation of phenol.

4.3.4 Kinetics of degradation

Photocatalytic degradation kinetics was studied for a phenolic solution with prepared RZ catalysts as shown in figure4.10 (d). The observation was carried out at 0.01M phenol concentration with a catalyst loading of 0.1mg/ml. For the low phenolic concentration, Langmuir-Hinshelwood first-order kinetic reaction was followed (Dresselhaus M.S.,et al.2010) and can be expressed in the following manner:-

$$In(C_0 / C) = kt \quad \text{---------- (4.9)}$$

where k is the degradation reaction rate constant in min^{-1} C_0 is the initial concentration, t is the reaction time and C is the concentration at time t. The values

of $In(C_t / C_0)$ were plotted against the time t in minutes as shown in figure4.10 (d).

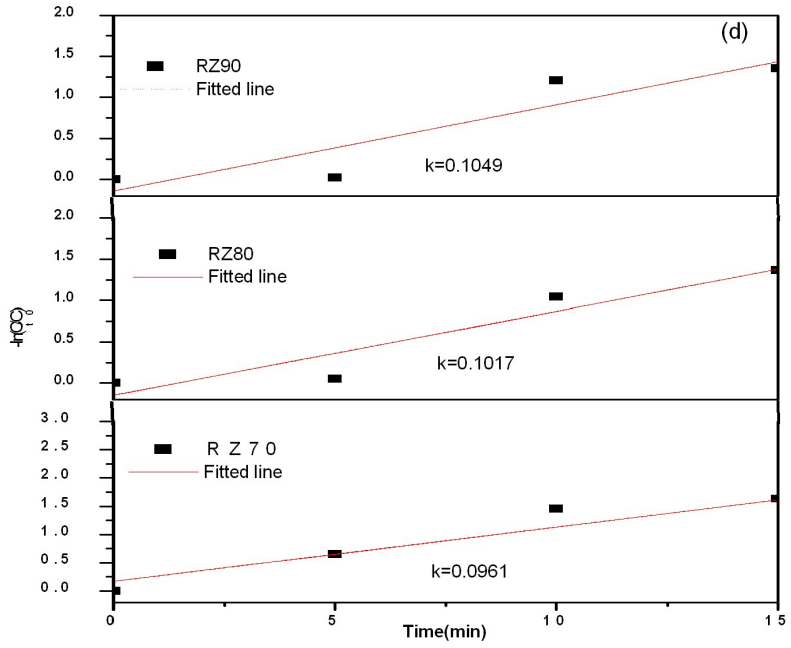

Figure 4.10 (d) Kinetic plots of RZ70, RZ80, and RZ90.

The reaction rate constant (k) was calculated through a linear fitting for the degradation of phenol in the presence of RZ catalysts. It can be seen from the results that RZ composites have rate constant (k = 0.0961min^{-1}), (k = 0.1017min^{-1}), (k = 0.1040min^{-1}) for RZ70, RZ80, RZ90 respectively, which showing best photocatalytic activity than that of the pure ZnO (k = 0.050min^{-1}) (F.Wang, et al.2018).The enhanced photocatalytic activity of RZ composites is due to surface to volume ratio of lotus-like ZnO on rGO sheets, which reconstructed atom arrangement and electrons states on specific configuration surface. During organic water pollutant remediation process, the radicals play an important role in the degradation of organic molecules. In the photocatalytic reaction, the oxygen on the surface of the rGO helps in the formation of O_2^- by capturing the energetic electrons

present in the rGO as stated in Eq. (4.13). The O_2^- then reacts with H_2O, present in the reaction medium, yielding highly active H_2O radicals Eq.(4.14). These active radicals further react with H^+ and generate (.OH) radicals (E.Grabowska,et al.2012). The generations of hydroxyl radicals (.OH) during the photocatalytic activity are a key step for photocatalytic degradation of the phenol (G.Darabdhara,et al.2016,S.K.Al-Dawery,et al.2019). The (.OH) radicals attack either phenol or phenolic compounds, and there is the formation of phenoxyl radicals, which are finally converted into their corresponding organic acid (S.K. Al-Daweryet, al.2019, L.G.Devi,et al.2019). The mechanism can be explained by the following reactions-

$$ZnO + h\nu \xrightarrow{sunlight} ZnO\ (e^- + h^+) \text{ ---------- (4.10)}$$

$$ZnO\ (e^-) + rGO \rightarrow ZnO + rGO\ (e^-) \text{ ---------- (4.11)}$$

$$ZnO\ (h^+) + OH^- \rightarrow ZnO + .OH \text{ ---------- (4.12)}$$

$$rGO\ (e^-) + O_2 \rightarrow rGO + .O2^- \text{ ---------- (4.13)}$$

$$rGO\ (e^-) + .O2^- + H_2O + H^+ \rightarrow rGO + H_2O_2 \text{ ---------- (4.14)}$$

$$rGO\ (e^-) + H_2O_2 \rightarrow rGO + .OH + OH^- \text{ ---------- (4.15)}$$

$$.OH + Phenol \rightarrow \text{degradation product} \text{ ---------- (4.16)}$$

The photocatalytic activity performance of different morphology of ZnO with rGO in previous literature and our present work is listed in table 4.2.

Table 4.2 Comparative study of degradation efficiency of rGO-ZnO based Photocatalyst

Photocatalysts	Synthesis Method	Catalyst loading ($mg\text{-}L^{-1}$)	Dye	Light source	Irradiation times (min	Degradation efficiency (%)	Reff.
rGO –ZnO	Dispersion	50	Methylene blue	Xe lamp 200W	50min	80%	Fu D. et al.2012
rGO –ZnO nanorods	Hydrothermal	50	Rhodamine B& phenol	300 W Xe arc lamp	12min	97.2%	Wang, F. et al.2018
rGO –ZnO sphere	Facile &microwave	0.2	Methylene blue	Visible irradiation	90min		Tien H.N. et al. 2013
rGO –ZnO nanowire	Facile	20	Rhodamine 6G	Mercury lamp 150W	10min	98%	Zhang, C. et al. 2014
rGO –ZnO Quantum dots	Chemical Route	3	Rhodamine 6G	100W UV lamp	45min	100 %	Mandals S.K. et al. 2019
ZnO flower/RGO	One-Pot Hydrothermal	50	Methylene blue	UV lamp 100W& Sunlight	150min	97%	Xu, S. et al. 2014
ZnO hierarchical Mesoporous flower /rGO	Hydrothermal	50	Methylene blue	300W Mercury-Xenon lamp		99%	A.Shanmugas-undaram, et al. 2018
ZnO lotus like/rGO Composites at 70 ^{0}C	Sol-gel	0.1	phenol	Sunlight	20 min	86 %	Present study

Dongying Fu et al. et al.2019 reported that the band gap of ZnO in ZnO-GO composites is small as compared to pure ZnO. The low content of catalyst could not absorb the light completely, and an excess amount of catalyst reflects the light. It was also reported that 50mg concentration of catalyst had good photocatalytic performance. Fengzhi Wang et al.2018 reported that 50mg catalyst concentration with nanorods like morphology of ZnO with rGO composites enhanced the photocatalytic performance in 12min due to the superior nature of nanorods. H.N.Tienet al.2013 reported that 0.2mg catalyst concentration of sphere-like morphology of ZnO

(ZnOSPs) composites with rGO enhanced the photocatalytic performance of methylene blue in 120min due to high surface area and a narrow band gap of rGO-ZnOSP as compared to the pure ZnO. C. Zhanget al.2014 reported that 20mg catalyst concentration of rGO-ZnO nano-wire enhanced photocatalytic performance and decomposes over 98% Rhodamine 6G due to the increased electron migration efficiency of the rGO-ZnO nanowire. S. K. Mandal et al. al.2019) reported that rGO-ZnO quantum dots photocatalytic materials enhanced the photocatalytic efficiency due to large surface to volume ratio of catalyst particles. S. Xuet al.2014 reported that 50mg catalyst concentration of flower-like ZnO-rGO nanocomposites enhanced the photocatalytic performance due to suppressing photogenerated carrier's recombination. A.Shanmugasundaramet al.2018 reported that 50mg hierarchical mesoporous flower-like zinc oxide with rGO composite catalyst concentration was an excellent photocatalytic performer in 2h. From the above literature study, we conclude that for the degradation of organic pollutant, the morphology of ZnO is very important.

On comparing literature studies with our present work, the lower catalytic concentration with lotus-like morphology formed by self-assembly of a large number of nanorodsenhanced the photocatalytic activity in minimum time. Two factors can explain this; first factor is due to lotus-like-ZnO structures, containing numerous ZnOnanorods, resulted in the high surface to volume ratio. This combination improved photocatalytic activity of RZ composites. The second factor was that visible light absorption of RZ composite is increased with rGO content effected the charge transfer by adjusting energy levels among the phenol, rGO, and ZnO.

4.3 Summary of Result

It is concluded that the inverted lotus-like structures prepared at temperature 70^0C by the sol-gel method, performed better photocatalytic activities. With a small degree variation in temperature during processing, the assembly of inverted lotus-like morphology was randomized, which was further self-assembly together to form straight lotus type morphology. The results of characterization techniques indicated the improvement in the crystalline quality and degree of reduction of RZ composite. It is also concluded that temperature influenced the assembly of lotus-like ZnO morphologies with variation in sizes. These morphologies in the nano-scale range were successfully decorated on the surfaces of rGO sheets along within their interlayer spaces. The results presented herein would have important consequences in the photocatalytic removal of phenol due to lotus-like ZnO morphology which enhances the photocatalytic activities under sunlight irradiation and results in maximum degradation efficiency 86% in 20min.